Article

Detection of Phenylalanine by Iridium Nanoclusters Using Time-Dependent Density Functional Theory Calculations

Published as part of ACS Omega special issue "Celebrating the 25th Anniversary of the Chemical Research Society of India".

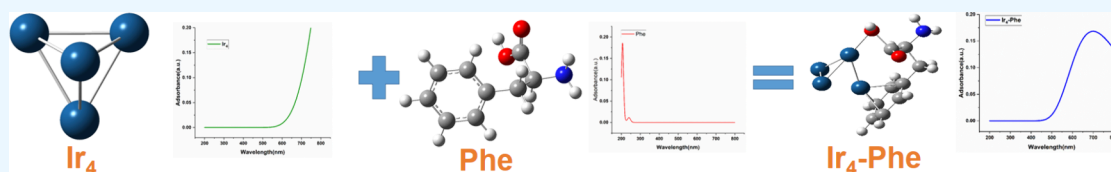Neelam Agrawal, Ashok Singh Bahota, Areeba Khan, Rajni Chaudhary, Keshav Kumar Singh, and Poonam Tandon*

Read Online

ACCESS | Metrics & More | Article Recommendations | SI Supporting Information

ABSTRACT: Metal nanoclusters have several applications in biological processes, medicine, cancer therapy, catalysis, etc. Iridium (Ir) nanoclusters exhibit excellent detection behavior compared to their bulk material. This work includes a deep insight into the interaction of Ir nanoclusters of four atoms (Ir_4) with amino acids and the analysis of Ir−amino acid (Ir−AAc) complexes. UV−visible spectroscopy of the Ir_4 nanocluster, amino acids, and their complexes was discussed as a way to detect amino acids with the help of the Ir_4 nanocluster. In UV−visible analysis, the UV−visible peak of phenylalanine (Phe) appeared at 204 nm with an excitation energy of 6.02 eV with a 0.0516 oscillator strength. Meanwhile, only in the Ir_4 nanocluster−phenylalanine (Ir−Phe) complex, the UV−visible peak was observed at 661 nm with an excitation energy of 1.87 eV and oscillator strength of 0.0051. This peak was observed due to the transition from HOMO−1 to LUMO+3. In the other complexes, no UV−visible peaks are observed. Thus, the results predict that the Ir_4 nanocluster can be used in the detection of Phe via UV−visible spectra.

INTRODUCTION

Nanomaterials can be distinguished on the basis of their physical and chemical properties, which mainly depend on their size, shape, surface area, and composition. Their unique and enhanced properties have led to numerous applications in various fields, such as nanobiotechnology, cancer therapy development, phase engineering, energy storage, detection, and sensors.[1−6] Metal nanoclusters are a category of nanomaterials consisting of a small number of metallic atoms, typically ranging from a few to several hundred. The size of the nanocluster is in the range of 2 to 100 nm. Unlike their bulk materials, nanoclusters have different electronic, optical, magnetic, and mechanical properties. The small size of nanoclusters makes them efficient catalysts for reactions including hydrogenation, oxidation, and carbon dioxide reduction.[7−16] The pressure can be used to control and manipulate the optical properties of the metal nanoclusters. Pressure-dependent optical absorption spectra of silver and gold nanoclusters offer valuable insights into their optical properties and behavior under different environmental conditions.[17] Boron nanoclusters have been demonstrated as effective adsorbents for heavy metals in aqueous environments. These materials have the potential to be used in a variety of

applications, including wastewater treatment and remediation.[18]

For several years, the structure, geometry, and possible application of clusters made up of various metals have been investigated, and iridium nanoclusters are one of these. Iridium is a nontoxic substance known for its high melting point, corrosion resistance, low reactivity, and biocompatibility. Iridium has drawn the attention of researchers due to its wide range of applications, including jewelry, medical devices, automotive catalysis, electrocatalysis, catalytic reactions, molecular imaging, and energy storage devices.[19−21] There are many research groups working on nanoclusters, and some are discussed here. Yonezawa et al.[22] studied the Ir nanocluster and reported that with increasing cluster size and mono oxide (MO) coverage, the adsorption energy of MO with the Ir cluster increases, suggesting that larger Ir clusters and higher MO coverage are more conducive to MO adsorption. Their

works are in brief about the dependency of the Ir cluster's stability on MO absorption, which is crucial information for developing and improving Ir-based catalysts and sensors. Tomihara et al.[23] reported on anions clusters of iridium oxide $Ir_nO_m^-$ (n = 5−8 and m = 0−14). Their work gives a detailed description of the evolution and binding modes of oxygen atoms and the motif of the iridium framework as a function of m through ion mobility mass spectrometry and theoretical calculations. The $Ir_nO_m^-$ (n ≥ 8 and m = 0−14) clusters have high structural diversity due to smaller surface energy. The small iridium oxide cluster has significant importance in establishing the structure−catalysis correlation, which is essential for designing and optimizing its catalytic performance. Kong et al.[24] have prepared a new type of dual-emitting gold nanoclusters (d-Au NCs) for the detection of phenylalanine and Fe^{3+}. Dual-emitting gold nanoclusters have an average decay time of 5.8 μs for 430 nm and 10 μs for 600 nm emission. The dual-emitting gold nanocluster particle size is uniform; and the diameter is 1.75 ± 0.3 nm, and it represents two different species simultaneously. Therefore, the prepared gold nanocluster detects two different species (phenylalanine and Fe^{3+}). D-Au NCs show a higher detection efficiency compared to single-emission metal clusters. Shang et al.[25] work on water-soluble fluorescent Ag nanoclusters as fluorescent sensors for Cu^{2+}. Due to paramagnetic properties via electron transfer, Cu^{2+} is a highly efficient fluorescence quencher. For the detection of Cu^{2+}, Ag nanoclusters are capable of detecting at low concentrations. The preparation of the fluorescent Ag nanocluster consisted of photoreduction and mixing of silver salt and PMAA (poly methacrylic acid). The absorption spectrum of the PMAA-Ag nanocluster shows a possible quenching mechanism of energy transfer between Ag and Cu^{2+}. Therefore, the Ag nanocluster is used as a sensor for Cu^{2+}.

In this work, we used an iridium nanocluster to detect amino acids with the help of UV−visible spectroscopy. Phenylalanine is an essential amino acid. The critical role of phenylalanine amino acid supplements is in treating the central nervous system. It is also used for depression, Parkinson's disease, chronic pain, osteoarthritis, rheumatoid arthritis, alcohol withdrawal symptoms, and vitiligo skin disease. Additionally, plants utilize phenylalanine to synthesize proteins and shield their skin from the damaging effects of ultraviolet light.[26−32]

■ COMPUTATIONAL DETAILS

In our work, we have chosen the stable iridium nanocluster with the least number of atoms, i.e., 4 (Ir_4), whose geometrical structure (i.e., pyramidal structure) was already reported by El-Bayyari et al.[33] All quantum chemical calculations were performed by Gaussian 16[34,35] software. To select the best method for the calculation of the Ir_4 nanocluster, we chose some methods that have already been used for the optimization of nanoclusters. We have optimized the Ir_4 nanocluster with the B3LYP, CAM-B3LYP, MN15, M062X, MP2, and CCSD methods with the LanL2DZ basis set. Further, the HOMO−LUMO gaps[36−38] obtained from these methods are compared in Figure 1 and Table S1, as the HOMO−LUMO energy gap is an important characteristic for the stability of molecules. It was observed that the HOMO−LUMO gaps corresponding to the MP2 and CCSD methods were similar (E_g = 7.82 eV). Thus, these two methods show the most appropriate candidature for this research work. As the CCSD method is computationally expensive, we opted for the
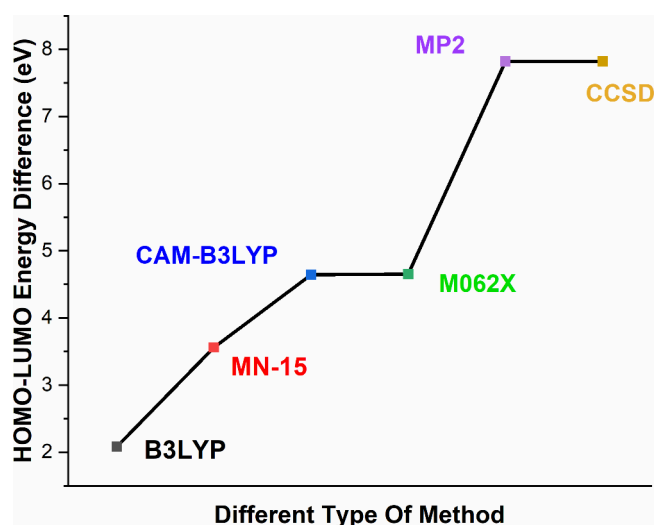

Figure 1. HOMO−LUMO comparison of the Ir_4 nanocluster with different types of methods.

MP2 method for the quantum calculations. Hence, the initial structure of the Ir_4 nanocluster, amino acids, and their complexes (Ir_4 adsorbed amino acids) were optimized using the MP2/LanL2DZ level of theory.

The analytical frequency calculations of all structures were performed using the MP2/Lan2DZ level of theory to examine the nature of the stationary points. All of the investigated structures show positive analytical frequency, which implies that all of the optimized structures are true minima. Density functional theory (DFT) is commonly used for straightforward calculation of properties related to electron distribution such as charge transfer and electron density distribution in excited states. Time-dependent density functional theory (TD-DFT) is an extension of DFT, providing valuable information about molecules' ground-state electronic structure. TD-DFT is a widely used computational method for simulating UV−visible spectra of a molecular structure.[39−42] Tamm−Dancoff approximation has been considered to analyze the electronic absorption spectra of the Ir_4 nanocluster, amino acids, and Ir−AAc complexes via TD-DFT with the CAM-B3LYP/LanL2DZ level of theory. For the calculation of TD-DFT on the scale of accuracy, the order of methods CAM-B3LYP > PBE0 > B3LYP > PBE shows that CAM-B3LYP has been found to provide reasonably accurate predictions of excitation energies and UV−visible spectra for a wide range of molecular systems.[43,44]

■ RESULTS AND DISCUSSION

The UV−visible spectra offer insights into the absorption or transmission of light in the UV−visible part of the electromagnetic spectrum. This type of spectrum helps us to understand the optical characteristics of nanoparticles, transition metals, and highly conjugated organic compounds. The UV−visible spectrum encompasses the wavelength range of 200 to 800 nm. The ultraviolet region covers 200 to 400 nm, while the visible region spans from 400 to 800 nm.[45]

The electronic configuration of the Ir atom is $[Xe]\ 4f^{14}\ 5d^7\ 6s^2$. Therefore, it is clear that in the Ir atom there are three unpaired electrons in its outermost subshell, which allows it to form complex compounds. Thus, the Ir atom shows electrophilic behaviors. When an Ir_4 nanocluster is optimized as shown in Figure 2[A], the bond length between the Ir−Ir atom
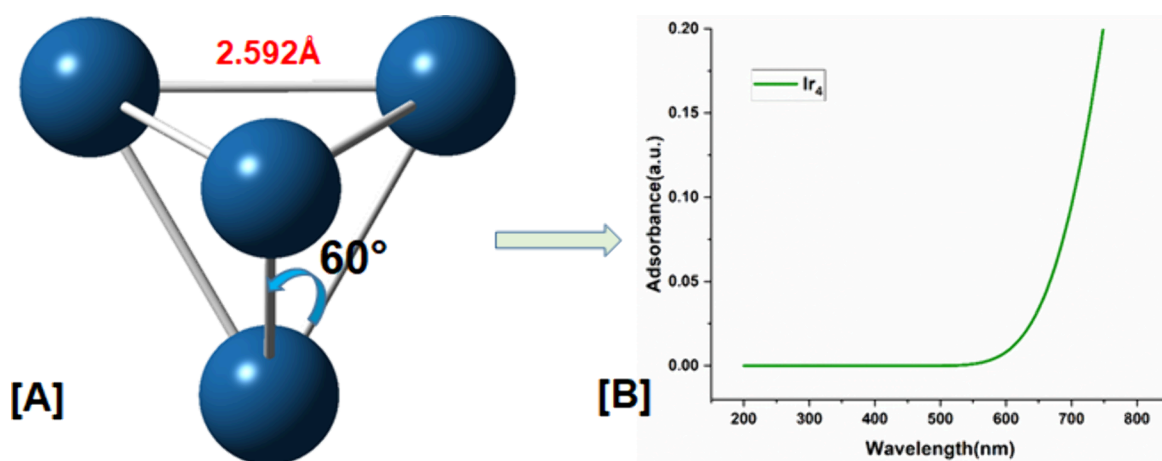
Figure 2. [A] Optimized structure of the Ir_4 nanocluster and [B] UV−visible spectra of the Ir_4 nanocluster.

Table 1. Theoretical UV−Visible Peak Positions (nm), Excitation Energies (eV), Oscillation Strengths, Major Contributions, and Experimental Reported UV−Visible Peak Positions (nm) of AAs and Ir_4-AAc Complexes Calculated at the CAM-B3LYP/LanL2DZ Level of Theory

Amino acids/ Complex	Theoretical observed wavelength (nm)	Excitation Energy (eV)	Oscillator Strength	Major contribution	Experimental reported wavelength (nm)
Alanine (Ala)	236	5.19	0.0037	H-1→LUMO (59%)	240[49]
Arginine (Arg)	214	5.74	0.0033	H-1→LUMO (69%)	210[50]
Asparagine (Asn)	207	5.93	0.0109	HOMO→LUMO (67%)	203[51]
Aspartic (Asp)	238	5.16	0.0045	HOMO→LUMO (49%)	227[52]
Cysteine (Cys)	212	5.79	0.0022	HOMO→LUMO (78%)	214[53]
Glutamic (Glu)	228	5.38	0.008	HOMO→LUMO (80%)	238[54]
Glutamine (Gln)	216	5.66	0.0037	HOMO→LUMO (77%)	227[52]
Glycine (Gly)	239	5.16	0.0006	H-1→LUMO (65%)	230[55]
Histidine (His)	234	5.27	0.0026	HOMO→LUMO (92%)	235[56]
Isoleucine (Ile)	242	5.11	0.003	H-1→LUMO (62%)	Not Found
Leucine (Leu)	241	5.11	0.0025	H-1→LUMO (54%)	235[57]
Lysine (Lys)	241	5.11	0.0031	H-2→LUMO (61%)	230[58]
Methionine (Met)	240	5.15	0.0093	H-1→LUMO (40%)	236[59]
Phenylalanine (Phe)	204	6.02	0.0516	HOMO→L+1 (45%)	209[60]
Proline (Pro)	229	5.37	0.0021	H-1→LUMO (72%)	226[61]
Serine (Ser)	209	5.88	0.0066	HOMO→LUMO (60%)	208[62]
Threonine (The)	211	5.83	0.0972	HOMO→LUMO (59%)	220[63]
Tryptophan (Trp)	245	4.97	0.027	H-4→L+1 (28%)	250[64]
Tyrosine (Tyr)	209	5.89	0.1315	HOMO→L+2 (70%)	200[65]
Valine (Val)	216	5.69	0.0092	HOMO→LUMO (59%)	220[66]
Ir−Phenylalanine	661	1.87	0.0051	H-1→L+3 (14%)	

is 2.592 Å, and the angle between Ir−Ir−Ir is 60° with a 3D pyramidal structure. The HOMO−LUMO energy gap is 7.820 eV, as provided in the Supporting Information, Table S2. The iridium atom interacts with three neighboring Ir atoms, forming a bond with the contribution of its valence electron. The electrons spread out over the entire cluster, forming metallic bonds that reduce the overall energy with increased stability. The tetrahedral arrangement allows each Ir atom to bond with three neighboring Ir atoms, resulting in a stable configuration. So, the Ir_4 nanocluster is more stable. The Ir4

nanocluster does not emit/absorb high energy photons. When the TD-DFT calculation is performed for Ir_4 nanoclusters, it is observed that there is no UV−visible peak in the UV−visible range. The UV−visible plot of the Ir_4 nanocluster is shown in Figure 2[B] while for the single atom spectrum it is obtained at 300 nm (given Supplementary Figure S1).

Amino acids show absorbance in different wavelength positions, depending on the presence of specific chromospheres in their molecular structure. These chromospheres are present in a side chain, which includes branches of hydro-
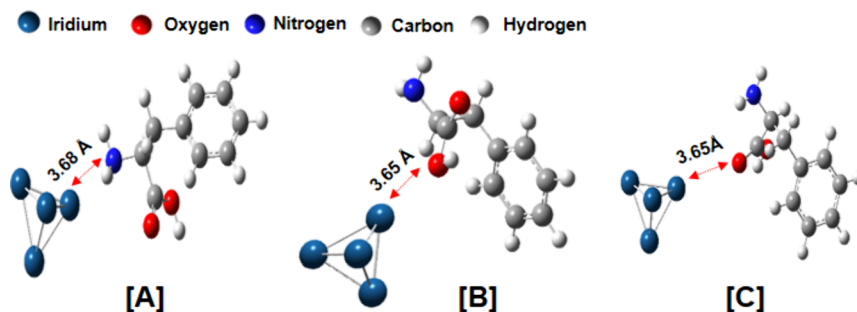
Figure 3. Initial input structure of all possible intact sides. [A] Ir_4 nanocluster with the $-NH_2$ group, [B] Ir_4 nanocluster with the $-OH$ group, and [C] Ir_4 nanocluster with the $-C=O$ group.
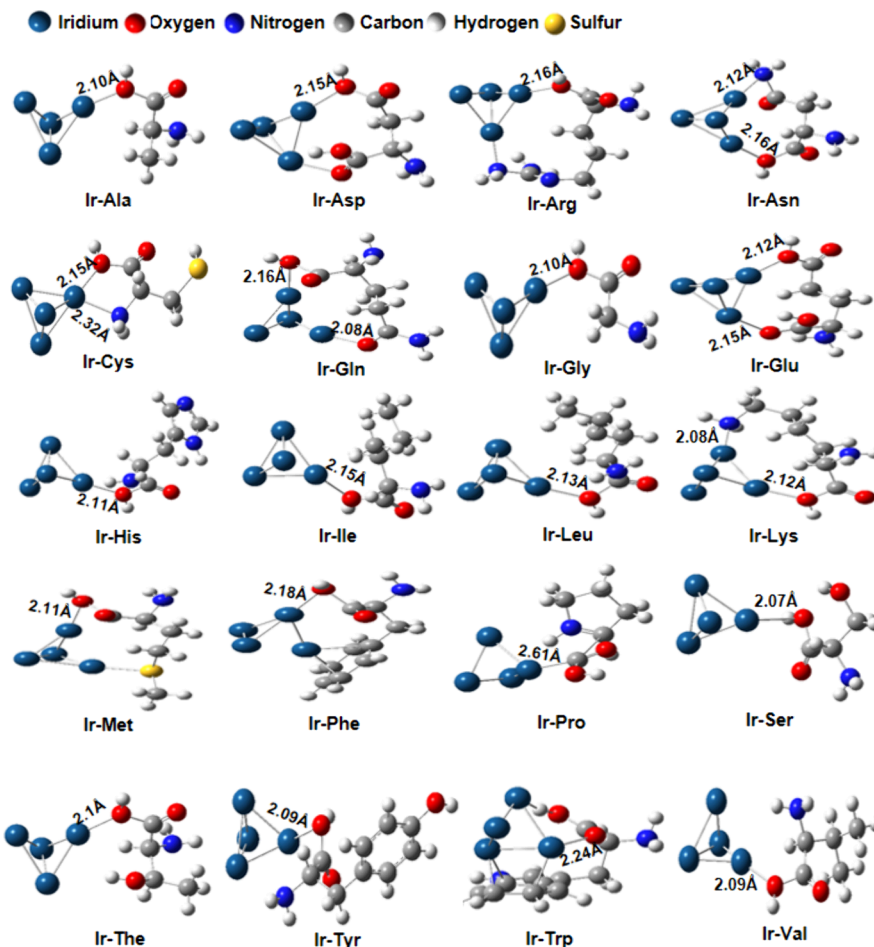

Figure 4. Optimized structures of Ir_4 nanocluster–amino acid (possible side with the $-OH$ group of the amino acid) complexes.

carbon, functional group, and aromatic ring (benzene ring). The UV region (200–320 nm) show the electronic absorption of amino acids.[46−48] The UV–visible peaks of all 20 basic amino acids (Ala, Arg, Asn, Asp, Cys, Glu, Gln, Gly, His, Ile, Leu, Lys, Met, Phe, Pro, Ser, The, Trp, Tyr, and Val) are observed in the 200–250 nm range. We have compared these (theoretically observed) UV–visible peaks of all of the amino acids with previously reported experimental data of pure amino acids. We have observed that theoretical UV–visible peaks of most amino acids (Histidine, Serine, Alanine, Arginine, Cysteine, etc.) have found the approximate same peak position as already reported in the experimental data. Therefore, we can say that the MP2/CAM-B3LYP level of theory provides nearly the same result as reported in the experimental research

papers. Theoretical observed UV–visible peak position, excitation energy, oscillator strength, major contribution, and experimentally reported peak position are in Table 1.

After optimizing the structure of the Ir_4 nanocluster and amino acids, we checked the Mulliken charges on them. We observed that at each corner atoms of the Ir_4 nanocluster have the same charge (zero charge). Therefore, Ir_4 nanoclusters have neutral behavior and show a strong interaction between the Ir–Ir atom. The Mulliken charge ranges present in the $-NH_2$, $-OH$, and $-C=O$ groups of amino acids are −0.42 to −0.61 eV, −0.47 to −0.50 eV, and −0.22 to −0.26 eV, respectively, in most of the amino acids. Both $-NH_2$ and $-COOH$ groups in amino acids are negatively charged, while in other amino acids both groups show different properties. It
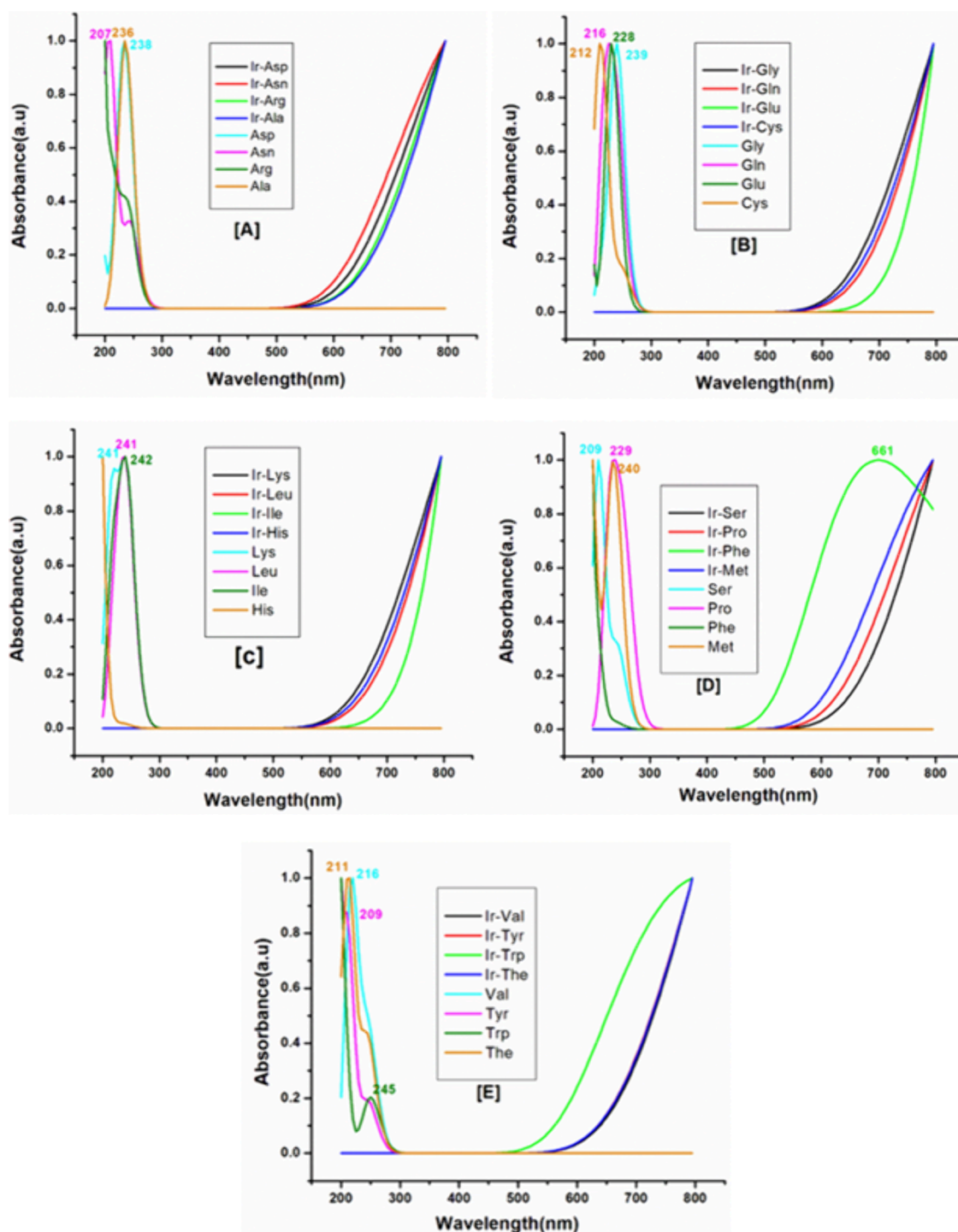
Figure 5. [A−E] UV−visible spectra graphs of pure amino acids and amino acid−Ir$_4$ nanocluster complexes.

is clear that amino acids show both behavior nucleophilic and electrophilic nature with different sides. Therefore, we have considered interaction of the Ir$_4$ nanocluster with −NH$_2$, −OH, and −C≡O groups of amino acids. We have shown examples of the initial input structure of all possible sides of the Ir$_4$ nanocluster−amino acid complexes (Ir−AAs complexes), which are shown in Figure 3. The initial distance between the nitrogen atom of the −NH$_2$ group and the iridium atom of the Ir$_4$ nanocluster is 3.68 Å (sum of the van der Waals radius of nitrogen and iridium). The initial distance between the oxygen atom of the −COOH group of the amino acid and

the iridium atom of the Ir$_4$ nanocluster is 3.65 Å (sum of the van der Waals radius of oxygen and iridium).

After the interaction of Ir$_4$ nanocluster with amino acids, the distances between the Ir atom and −OH, −C≡O, and −NH$_2$ groups of amino acids are decreased and are approximately in the 2.07−2.61 Å, 2.02−2.40 Å, and 2.07−2.40 Å ranges, respectively. Therefore, we can say they are attracted to each other and form complexes. In the interaction of the Ir$_4$ nanocluster with amino acid, the Ir−Ir bond length of the Ir$_4$ nanocluster also changes. These changes are detailed in Supplementary Table S3. The optimized structure of the
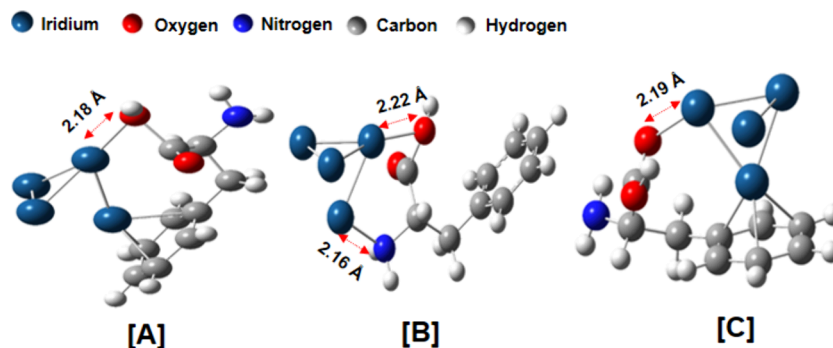
Figure 6. Optimized structures of the Ir−Phe complex with the sides of [A] −OH, [B] −NH$_2$, and [C] −C═O.

complexes with the bond distance of the interaction side is shown in Figure 4 (Ir$_4$ nanocluster with the −OH group of the carboxylic group), Figure S2 (Ir$_4$ nanocluster with the −NH$_2$ group), and Figure S3 (Ir$_4$ nanocluster with the oxygen atom of the carboxylic group).

The excited state of the complexes involved in absorption can be calculated through TD-DFT. We used these excited states to simulate the UV−visible spectrum of the Ir$_4$ nanocluster, pure amino acids, and Ir$_4$-amino acids complexes. The UV−visible spectra of the pure amino acids and amino acid absorbed Ir$_4$ nanocluster are shown in Figure 5. In the amino acids, only Phe has aromatic R-groups and the lowest excitation energy 6.02 eV compared to other amino acids as shown in Table 1. Due to the presence of a benzene ring in these amino acids, they have an n → π^* transition present. Being hydrophobic and having an aromatic ring structure, phenylalanine is an important amino acid that is categorized as an aromatic amino acid due to its strong interaction. In the Phe and Trp amino acids, they interact with the Ir$_4$ nanocluster with two side benzene rings and −COOH group as shown in Figure 4 and Figures S1 and S2. The bond lengths between the Ir atom and −OH in the Ir−Phe and Ir−Trp complexes are 2.18 and 2.24 Å, respectively, and are shown in Figure 4. Therefore, the interaction between the Ir$_4$ nanocluster and Phe amino acid is stronger than that of the Ir−Trp complex. Due to this effect, internal bonding is affected. Thus, the Ir$_4$ adapts to a different type of structure after breaking from its initial structure.

After adsorption of the amino acids on the Ir$_4$ nanocluster, only the Ir−Phe complex has shown the UV−visible peak in the UV−visible region (400−800 nm), while other complexes have observed no peak in the UV−visible region as shown in Figure 5. The pure phenylalanine (Phe) shows a UV−visible peak at 204 nm with 6.02 eV excitation energy. The optimized structures are shown in Figure 6 for the cases of the Ir$_4$ nanocluster interacting with the sides of an −NH$_2$ group and −COOH group of Phe.

The Ir−Phe complex has 1.49 and 1.47 eV excitation energies with 0.0011 and 0.0001 oscillation strengths with the sides of an −NH$_2$ group and −C═O group, respectively. The peaks of the Ir−Phe complex are not shown in the UV−visible region due to the interaction with the side of the −NH$_2$ group and −C═O group. Meanwhile Ir$_4$ interacts with the −OH side of Phe, and the Ir−Phe complex has an excitation energy 1.87 eV with a 0.0051 oscillation strength. When we compared the adsorption energies of the Ir$_4$ nanoclusters with −C═O, −OH, and −NH$_2$ groups, it was observed that the Ir$_4$ nanocluster showed the maximum absorption energy with

the −OH group (given the information in Supplementary Table S4). Therefore, after interaction of the Ir$_4$ nanocluster with Phe, the UV−visible peak of the Ir−Phe complex has a 661 nm red shift with 4.89 eV adsorption energy shown in Figure 5[D]. As shown in Figure 7, pure Ir$_4$ nanoclusters have
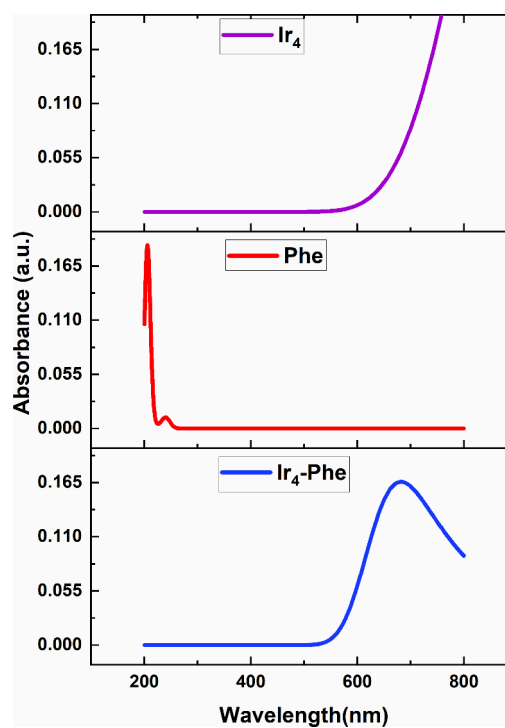

Figure 7. Comparison UV−visible plots of the Ir$_4$ nanocluster, Phe amino acid, and Ir−Phe complex.

no peak in the UV−visible region. Phe has a peak at 204 nm with a 0.0516 oscillator strength in the UV−visible region. After the interaction, the Ir−Phe complex shows a peak at 661 nm with an 0.0051 oscillator strength. This peak is shown as a consequence of the transition from the Ir$_4$ nanocluster with different HOMO−LUMO orbitals. This transition occurs due to the transition of H-1→L+3 (14%).

■ CONCLUSION

In this work, we selected the smallest stable Ir$_4$ nanocluster. We have studied the optimized structure of the Ir$_4$ nanocluster, pure amino acids, and complexes of Ir−amino acids with the help of the MP2/LanL2DZ level of theory. After the optimization, TD-DFT was used to understand the UV−

visible adsorption properties. In the UV−visible spectra of the Ir$_4$ nanocluster and its complexes with amino acids, calculations were performed with the help of CAM-B3LYP/LanL2DZ. We found that the Ir$_4$ nanocluster has no peak in the UV−visible spectra. Meanwhile, the peaks are observed between the range 200−250 nm in the amino acids. With analysis of the UV−visible spectra of the formed complexes, we observed that only the Ir−Phe complex has a peak at 661 nm with a 0.4721 oscillator strength, which is suitable for the experimental observation. Therefore, the Ir$_4$ nanocluster can be used as a Phe amino acid detector. As a result of our research, we are able to identify the Phe amino acid in mixtures of two or more amino acids.

■ ASSOCIATED CONTENT

ⓈⒾ Supporting Information

The Supporting Information is available free of charge at https://pubs.acs.org/doi/10.1021/acsomega.4c05684.

> HOMO−LUMO comparison of Ir$_4$ nanocluster with different types of methods; geometrical information on the optimized iridium nanocluster (Ir$_4$); after the interaction of the Ir$_4$ nanocluster with amino acids, the Ir−Ir bond length of the Ir$_4$ nanocluster; comparison of interactions of the Ir−Phe complex (Ir$_4$ nanocluster−phenylalanine amino acid) with different sides; images of the optimized structure of the Ir$_4$ nanocluster amino acid complexes with the side of −NH$_2$ group; and images of the optimized structure of the Ir$_4$ nanocluster amino acid complexes with the side of −C═O (PDF)

■ AUTHOR INFORMATION

Corresponding Author

Poonam Tandon − *Department of Physics, University of Lucknow, Lucknow 226007 Uttar Pradesh, India; Vice Chancellor in Deen Dayal Upadhyaya Gorakhpur University, Gorakhpur 273009 Uttar Pradesh, India;* ⓞ orcid.org/0000-0002-8120-0498; Email: tandon_poonam@lkouniv.ac.in

Authors

Neelam Agrawal − *Department of Physics, University of Lucknow, Lucknow 226007 Uttar Pradesh, India*

Ashok Singh Bahota − *Department of Physics, University of Lucknow, Lucknow 226007 Uttar Pradesh, India*

Areeba Khan − *Department of Physics, University of Lucknow, Lucknow 226007 Uttar Pradesh, India*

Rajni Chaudhary − *Department of Physics, University of Lucknow, Lucknow 226007 Uttar Pradesh, India*

Keshav Kumar Singh − *Department of Physics, University of Lucknow, Lucknow 226007 Uttar Pradesh, India*

Complete contact information is available at:
https://pubs.acs.org/10.1021/acsomega.4c05684

Author Contributions

Neelam Agrawal: conceptualization, data curation, formal analysis, investigation, methodology, validation, writing original draft and plotting of figures. **Ashok Singh Bahota:** conceptualization, writing review and editing. **Areeba Khan:** introduction and methodology. **Rajni Chaudhary:** introduction and methodology. **Keshav Kumar Singh:** writing−review and editing. **Poonam Tandon:** resources, software, supervision, validation, and visualization.

Notes

The authors declare no competing financial interest.

■ ABBREVIATIONS

Ir, Iridium; Ir4, Iridium nanocluster of four atoms; Ir−Aac, Iridium−amino acids; Ala, Alanine; Arg, Arginine; Asn, Asparagine; Asp, Aspartic; Cys, Cysteine; Gln, Glutamine; Glu, Glutamic; Gly, Glycine; His, Histidine; Iso, Isoleucine; Leu, Leucine; Lys, Lysine; Met, Methionine; Phe, Phenylalanine; Pro, Proline; Ser, Serine; The, Threonine; Trp, Tryptophan; Tyr, Tyrosine; Val, Valine; UV−visible, Ultraviolet−visible; HOMO, Highest occupied molecular orbital; LUMO, Lowest unoccupied molecular orbital

■ REFERENCES

(1) Baig, N.; Kammakakam, I.; Falath, W. Nanomaterials: A review of synthesis methods, properties, recent progress, and challenges. *Mater. Adv.* **2021**, 2, 1821−1871.

(2) Chen, Y.; Lai, Z.; Zhang, X.; Fan, Z.; He, Q.; Tan, C.; Zhang, H. Phase engineering of nanomaterials. *Nat. Rev. Chem.* **2020**, 4 (5), 243−256.

(3) Cheng, Z.; Li, M.; Dey, R.; Chen, Y. Nanomaterials for cancer therapy: current progress and perspectives. *J. Hematol. Oncol.* **2021**, 14, 85.

(4) Saleh, T. A. Nanomaterials: Classification, properties, and environmental toxicities. *Environ. Technol. Innov.* **2020**, 20, 101067.

(5) Pomerantseva, E.; Bonaccorso, F.; Feng, X.; Cui, Y.; Gogotsi, Y. Energy storage: The future enabled by nanomaterials. *Science* **2019**, 366, eaan8285.

(6) Zeng, L.; Wei, X. F.; Liang, M. K.; Zhao, J.; Zhu, B. C. Probing on the Stable Structure of Silicon-Doped Charged Magnesium Nanomaterial Sensor: SiMgn ± 1 (N = 2−12) Clusters DFT Study. *Front. Mater.* **2020**, DOI: 10.3389/fmats.2020.00221.

(7) Padash, R.; Rahimi-Nasrabadi, M.; Shokuhi Rad, A.; Sobhani-Nasab, A.; Jesionowski, T.; Ehrlich, H. A comparative computational investigation of phosgene adsorption on (XY) 12 (X= Al, B and Y= N, P) nanoclusters: DFT investigations. *J. Clust. Sci.* **2019**, 30, 203−218.

(8) Rosi, N. L.; Mirkin, C. A. Nanostructures in biodiagnostics. *Chem. Rev.* **2005**, 105, 1547−1562.

(9) Liu, X.; Yuan, J.; Yao, C.; Chen, J.; Li, L.; Bao, X.; Yang, J.; Wu, Z. Crystal and solution photoluminescence of MAg24 (SR) 18 (M= Ag/Pd/Pt/Au) nanoclusters and some implications for the photoluminescence mechanisms. *J. Phy. Chem. C* **2017**, 121 (25), 13848−13853.

(10) Bahota, A. S.; Singh, K. K.; Kumar, R.; Tandon, P. Ab-initio simulation of the interaction of gold nanoclusters with glycine. *J. Mol. Struct.* **2022**, 1266, 133447.

(11) Akanuma, Y.; Imaoka, T.; Sato, H.; Yamamoto, K. Silver in the Center Enhances Room-Temperature Phosphorescence of a Platinum Sub-nanocluster by 18 Times. *Angew. Chem.* **2021**, 133, 4601−4604.

(12) Lei, Z.; Wan, X.-K.; Yuan, S.-F.; Guan, Z.-J.; Wang, Q.-M. Alkynyl Approach toward the Protection of Metal Nanoclusters. *Acc. Chem. Res.* **2018**, 51, 2465−2474.

(13) Krishna Kumar, A. S.; Tseng, W. L. Perspective on recent developments of near infrared-emitting gold nanoclusters: Applications in sensing and bio-imaging. *Anal. Methods* **2020**, 12, 1809−1826.

(14) Porret, E.; Le Guével, X.; Coll, J. L. Gold nanoclusters for biomedical applications: Toward: In vivo studies. *J. Mater. Chem. B* **2020**, 8, 2216−2232.

(15) Jalili, R.; Dastborhan, M.; Chenaghlou, S.; Khataee, A. Incorporating of gold nanoclusters into metal-organic frameworks for highly sensitive detection of 3-nitrotyrosine as an oxidative stress biomarker. *J. Photochem. Photobiol. A Chem.* **2020**, *391*, 112370.

(16) Loginova, A. S.; Savintseva, L. A.; Ignatov, S. K. Structure and electronic excitation spectra of low-lying isomers of Aun clusters (n = 2−20). A DFT study. *Comput. Theor. Chem.* **2019**, *1170*, 112637.

(17) Li, Q.; Mosquera, M. A.; Jones, L. O.; Parakh, A.; Chai, J.; Jin, R.; Schatz, G. C.; Gu, X. W. Pressure-induced optical transitions in metal nanoclusters. *ACS Nano* **2020**, *14* (9), 11888−11896.

(18) Milon; Hossain, M. K.; Roy, D.; Ahmed, F. Boron nanocluster as a heavy metal adsorbent in aqueous environment: A DFT Study. *J. Mol. Struct.* **2021**, *1237*, 130302.

(19) Xiao, M.; Zhu, J.; Li, G.; Li, N.; Li, S.; Cano, Z. P.; Ma, L.; Cui, P.; Xu, P.; Jiang, G.; Chen, Z.; et al. A single-atom iridium heterogeneous catalyst in oxygen reduction reaction. *Angew. Chem., Int. Ed.* **2019**, *58* (28), 9640−9645.

(20) Wang, Q.; Xu, C. Q.; Liu, W.; Hung, S. F.; Bin Yang, H.; Gao, J.; Cai, W.; Chen, H. M.; Li, J.; Liu, B. Coordination engineering of iridium nanocluster bifunctional electrocatalyst for highly efficient and pH-universal overall water splitting. *Nat. Commun.* **2020**, *11* (1), 4246.

(21) Karaman, A.; Boudjahem, A. G.; Boulbazine, M.; Gueid, A. Stability and electronic properties of IrnV (n = 2−10) nanoclusters and their reactivity toward N2H4 molecule. *Struct. Chem.* **2020**, *31*, 203−214.

(22) Yonezawa, A. F.; Nagurniak, G. R.; Orenha, R. P.; Silva, E. H. d.; Parreira, R. L. T.; Piotrowski, M. J. Stability Changes in Iridium Nanoclusters via Monoxide Adsorption: A DFT Study within the van der Waals Corrections. *J. Phys. Chem. A* **2021**, *125* (22), 4805−4818.

(23) Tomihara, R.; Koyasu, K.; Nagata, T.; Wu, J. W.; Nakano, M.; Ohshimo, K.; Misaizu, F.; Tsukuda, T. Structural Evolution of Iridium Oxide Cluster Anions Ir n O m−(n= 5−8) with Sequential Oxidation: Binding Mode of O Atoms and Ir Framework. *J. Phys. Chem. C* **2019**, *123* (24), 15301−15306.

(24) Kong, C.; Luo, Y.; Zhang, W.; Lin, T.; Na, Z.; Liu, X.; Xie, Z. A ratio fluorescence method based on dual emissive gold nanoclusters for detection of biomolecules and metal ions. *RSC Adv.* **2022**, *12* (19), 12060−12067.

(25) Shang, L.; Dong, S. Silver nanocluster-based fluorescent sensors for sensitive detection of Cu(ii). *J. Mater. Chem.* **2008**, *18*, 4636−4640.

(26) Li, D.; Kumari, B.; Makabenta, J. M.; Gupta, A.; Rotello, V. Effective detection of bacteria using metal nanoclusters. *Nanoscale* **2019**, *11*, 22172−22181.

(27) Dinu, A.; Apetrei, C. A Review of Sensors and Biosensors Modified with Conducting Polymers and Molecularly Imprinted Polymers used in Electrochemical Detection of Amino Acids: Phenylalanine, Tyrosine, and Tryptophan. *Int. J. Mol. Sci.* **2022**, *23* (3), 1218.

(28) Paizs, C.; Katona, A.; Rétey, J. The interaction of heteroaryl-acrylates and alanines with phenylalanine ammonia-lyase from parsley. *Chem. - A Eur. J.* **2006**, *12* (10), 2739−2744.

(29) Moja, E. A.; Lucini, V.; Benedetti, F.; Lucca, A. Decrease in plasma phenylalanine and tyrosine after phenylalanine-tyrosine free amino acid solutions in man. *Life Sciences* **1996**, *58* (26), 2389−2395.

(30) Mahalakshmi, R.; Jesuraja, S. X.; Das, S. J. Growth and characterization of L-phenylalanine. *Cryst. Res. Technol.* **2006**, *41*, 780−783.

(31) King, J. M.; Muthian, G.; MacKey, V.; Smith, M.; Charlton, C. L-Dihydroxyphenylalanine modulates the steady-state expression of mouse striatal tyrosine hydroxylase, aromatic L-amino acid decarboxylase, dopamine and its metabolites in an MPTP mouse model of Parkinson's disease. *Life Sci.* **2011**, *89*, 638−643.

(32) Zhai, G.; Sun, X.; Randell, E. W.; Liu, M.; Wang, N.; Tolstykh, I.; Rahman, P.; Torner, J.; Lewis, C. E.; Nevitt, M. C.; Guermazi, A.; Felson, D. T.; et al. Phenylalanine is a novel marker for radiographic knee osteoarthritis progression: the MOST study. *J. rheumatol.* **2021**, *48* (1), 123−128.

(33) El-Bayyari, Z.; Hamad, B. Embryonic Iridium nanoclusters (n = 3−13): A molecular dynamics computer simulation. *Int. J. Mod. Phys. C* **2019**, *30*, 2050002.

(34) Yu, H. S.; He, X.; Li, S. L.; Truhlar, D. G. MN15: A Kohn-Sham global-hybrid exchange-correlation density functional with broad accuracy for multi-reference and single-reference systems and noncovalent interactions. *Chem. Sci.* **2016**, *7*, 5032−5051.

(35) Marques, M. A. L.; Gross, E. K. U. Time-dependent density functional theory. *Annu. Rev. Phys. Chem.* **2004**, *55*, 427−455.

(36) Tahmasebi, E.; Shakerzadeh, E.; Biglari, Z. Theoretical assessment of the electro-optical features of the group III nitrides (B 12 N 12, Al 12 N 12 and Ga 12 N 12) and group IV carbides (C 24, Si 12 C 12 and Ge 12 C 12) nanoclusters encapsulated with alkali metals (Li, Na and K). *Appl. Surf. Sci.* **2016**, *363*, 197−208.

(37) Hohenstein, E. G.; Chill, S. T.; Sherrill, C. D. Exchange-Correlation the M05-2X and M06-2X Exchange-Correlation Functionals for Noncovalent Interactions. *J. Chem. Theory Comput.* **2008**, *4*, 1996−2000.

(38) Feyereisen, M.; Fitzgerald, G.; Komornicki, A. Use of approximate integrals in ab initio theory. An application in MP2 energy calculations. *Chem. Phys. Lett.* **1993**, *208*, 359−363.

(39) Schmid, F. X. Biological macromolecules: UV-visible spectrophotometry. *eLS* 2001.

(40) Skoog, D. A.; Holler, F. J.; Crouch, S. R. *Principles of Instrumental Analysis*; Cengage Learning: 2017.

(41) Chen, Z.; Dinh, H. N.; Miller, E. *Photoelectrochemical water splitting: standards, experimental methods, and protocols*; Springer: 2013; Vol. 344, pp 6−15.

(42) Förster, H. UV/VIS Spectroscopy. In *Characterization I. Molecular Sieves − Science and Technology*, Vol. 4; Karge, H. G., Weitkamp, J., Eds. Springer: Berlin, Heidelberg, 2004. DOI: 10.1007/b94239

(43) Jacquemin, D.; Perpète, E. A.; Ciofini, I.; Adamo, C. On the TD-DFT UV/vis spectra accuracy: The azoalkanes. *Theor. Chem. Acc.* **2008**, *120*, 405−410.

(44) Ali, A.; Rafiq, M. I.; Zhang, Z.; Cao, J.; Geng, R.; Zhou, B.; Tang, W. TD-DFT benchmark for UV-visible spectra of fused-ring electron acceptors using global and range-separated hybrids. *Phys. Chem. Chem. Phys.* **2020**, *22* (15), 7864−7874.

(45) Antosiewicz, J. M.; Shugar, D. UV−Vis spectroscopy of tyrosine side-groups in studies of protein structure. Part 2: selected applications. *Biophys. Rev.* **2016**, *8*, 163−177.

(46) Seracu, D. I. The study of uv and vis absorption spectra of the complexes of amino acids with ninhydrin. *Anal. Lett.* **1987**, *20*, 1417−1428.

(47) Kuipers, B. J. H.; Gruppen, H. Prediction of molar extinction coefficients of proteins and peptides using UV absorption of the constituent amino acids at 214 nm to enable quantitative reverse phase high-performance liquid chromatography-mass spectrometry analysis. *J. Agric. Food Chem.* **2007**, *55*, 5445−5451.

(48) Prasad, S.; Mandal, I.; Singh, S.; Paul, A.; Mandal, B.; Venkatramani, R.; Swaminathan, R. Near UV-Visible electronic absorption originating from charged amino acids in a monomeric protein. *Chem. Sci.* **2017**, *8* (8), 5416−5433.

(49) Caroline, M. L.; Sankar, R.; Indirani, R. M.; Vasudevan, S. Growth, optical, thermal and dielectric studies of an amino acid organic nonlinear optical material: l-Alanine. *Mater. Chem. Phys.* **2009**, *114*, 490−494.

(50) Kalaiselvi, D.; Kumar, R. M.; Jayavel, R. Single crystal growth and properties of semiorganic nonlinear optical L-arginine hydrochloride monohydrate crystals. *Cryst. Res. Technol.* **2008**, *43*, 851−856.

(51) Masilamani, S.; Ilayabarathi, P.; Maadeswaran, P.; Chandrasekaran, J.; Tamilarasan, K. Synthesis, growth and characterization of a novel semiorganic nonlinear optical single crystal: L-Asparagine cadmium chloride monohydrate. *Optik (Stuttg).* **2012**, *123*, 1304−1306.

(52) Yogam, F.; Vetha Potheher, I.; Jeyasekaran, R.; Vimalan, M.; Arockiaraj, M. A.; Sagayaraj, P. Growth, thermal, and optical

properties of l-asparagine monohydrate NLO single crystal. *J. therm. Anal.calorim.* **2013**, *114*, 1153−1159.

(53) Biçer, E.; Qetinkaya, P. A voltammetric study on the interaction of novobiocin with cysteine: pH effect. *J. Chil. Chem. Soc.* **2009**, *54*, 46−50.

(54) Aarthi, J.; Dhanasekaran, P. Growth, structural, optical, thermal and dielectric properties of L-glutamic acid hydrochloride crystal for optoelectronic device applications. *J. Cryst. Growth* **2019**, *506*, 79−82.

(55) Chagas, M. A. S.; Galvão, A. D.; de Moraes, F. T.; Ribeiro, A. T. B. N.; de Siqueira, A. B.; de Assis Salama, I. C. C.; Arrais-Silva, W. W.; de Sousa, K. M. D.; de Sousa Pereira, C. C.; dos Santos, W. B. Synthesis Characterization and Analysis of Leishmanicide Ability of the Compound [Ru (Cl) 3 (H2O) 2 (gly)]. *Open J. Inor. Chem.* **2017**, *7* (4), 89−101.

(56) Gonsago, C. A.; Albert, H. M.; Malliga, P.; Arul Pragasam, A. J. Growth and characterization of pure and thiourea doped L-histidine single crystals. *Mater. Manuf. Process.* **2012**, *27*, 355−359.

(57) Adhikari, S.; Kar, T. Bulk single crystal growth and characterization of l-leucine - A nonlinear optical material. *Mater. Chem. Phys.* **2012**, *133*, 1055−1059.

(58) Ramesh Babu, R.; Vijayan, N.; Gopalakrishnan, R.; Ramasamy, P. Growth and characterization of L-lysine monohydrochloride dihydrate (L-LMHCl) single crystal. *Cryst. Res. Technol.* **2006**, *41*, 405−410.

(59) Mamun, M. A.; Ahmed, O.; Bakshi, P. K.; Ehsan, M. Q. Synthesis and spectroscopic, magnetic and cyclic voltammetric characterization of some metal complexes of methionine: [(C5H10NO2S)2MII]; MII = Mn(II), Co(II), Ni(II), Cu(II), Zn(II), Cd(II) and Hg(II). *J. Saudi Chem. Soc.* **2010**, *14*, 23−31.

(60) Wetlaufer, D. B. Ultraviolet spectra Of Proteins and Amino Acids. *Adv. Protein Chem.* **1963**, *17*, 303−390.

(61) Gupta, M. K.; Sinha, N.; Kumar, B. Growth and character-ization of new semi-organic l-proline strontium chloride monohydrate single crystals. *Phys. B Condens. Matter* **2011**, *406*, 63−67.

(62) Rajesh, K.; Kumar, P. P. Structural, Linear, and Nonlinear Optical and Mechanical Properties of New Organic L-Serine Crystal. *J. Mater.* **2014**, *2014* (2014), 1−5.

(63) Ramesh Kumar, G.; Gokul Raj, S.; Mohan, R.; Jayavel, R. Growth, structural and spectral analyses of nonlinear optical l-threonine single crystals. *J. Cryst. Growth* **2005**, *275*, e1947−e1951.

(64) Suresh, P.; Janarthanan, S.; Sugaraj Samuel, R.; Jestin Lenus, A.; Shanthi, C. Synthesis, growth and spectral, optical and thermal characterization studies on L-Tryptophan p-nitrophenol (LTPN) single crystals for NLO applications. *Spectrochim. Acta - Part A Mol. Biomol. Spectrosc.* **2015**, *135*, 732−735.

(65) Rava, R. P.; Spiro, T. G. Resonance enhancement in the ultraviolet Raman spectra of aromatic amino acids. *J. Phys. Chem.* **1985**, *89*, 1856−1861.

(66) Sangeetha, M. K.; Mariappan, M.; Madhurambal, G.; Mojumdar, S. C. TG−DTA, XRD, SEM, EDX, UV, and FT-IR spectroscopic studies of l-valine thiourea mixed crystal. *J. Therm. Anal. Calorim.* **2015**, *119*, 907−913.